HHS Public Access

Author manuscript

Magn Reson Med. Author manuscript; available in PMC 2017 July 01.

Published in final edited form as:

Magn Reson Med. 2016 July ; 76(1): 197–205. doi:10.1002/mrm.25858.

Robust Self-navigated Body MRI Using Dense Coil Arrays

Tao Zhang[1,2], **Joseph Y. Cheng**[1,2], **Yuxin Chen**[3], **Dwight G. Nishimura**[2], **John M. Pauly**[2], and **Shreyas S. Vasanawala**[1]

[1]Department of Radiology, Stanford University, Stanford, California

[2]Department of Electrical Engineering, Stanford University, Stanford, California

[3]Department of Statistics, Stanford University, Stanford, California

Abstract

Purpose—To develop a robust motion estimation method for free-breathing body MRI using dense coil arrays.

Methods—Self-navigating pulse sequences can measure subject motion without using external motion monitoring devices. With dense coil arrays, individual coil elements can provide localized motion estimates. An averaged motion estimate over all coils is often used for motion compensation. However, this motion estimate may not accurately represent the dominant motion within the imaging volume. In this work, a coil clustering method is proposed to automatically determine the dominant motion for dense coil arrays. The feasibility of the proposed method is investigated in free-breathing abdominal MRI and cardiac MRI, and compared with manual motion estimate selection for respiratory motion estimation and electrocardiography (ECG) for cardiac motion estimation.

Results—Automated motion estimation achieved similar respiratory motion estimation compared to manual selection (averaged correlation coefficient 0.989 and 0.988 for abdominal MRI and cardiac MRI respectively), and accurate cardiac triggering compared to ECG (averaged temporal variability 17.5 ms).

Conclusion—The proposed method can provide accurate automated motion estimation for body MRI using dense coil arrays. It can enable self-navigated free-breathing abdominal and cardiac MRI without the need for external motion monitoring devices.

Keywords

parallel imaging; motion correction; coil arrays; self-navigated MRI; abdominal MRI; cardiac MRI

Introduction

Patient motion remains one of the main sources for MRI artifacts. For body MRI, respiratory motion and cardiac motion are two major types of motion that can significantly degrade

Address correspondence to: Tao Zhang, Packard Electrical Engineering, Room 212, 350 Serra Mall, Stanford, CA 94305-9510, TEL: (650) 723-3810, tzhang08@stanford.edu.

image quality. While some fast imaging techniques can avoid respiratory motion by reducing the scan time to a breath-hold, some patients, such as young children and some diseased adults, cannot voluntarily suspend their respiration. Most clinical abdominal and cardiac MRI protocols consist of MRI sequences with long scan time that also require careful consideration of respiratory motion and cardiac motion (1).

External devices, such as respiratory bellows, electrocardiography (ECG) and plethysmography (PG), are usually applied to monitor these two types of motion. Using respiratory bellows, the acquired data can be ensured to fall within a similar respiratory state by respiratory triggering or gating (2). ECG is also widely utilized for cardiac gating/triggering (3–5). However, external motion monitoring devices require additional patient preparation time. They can also be ineffective in some cases. For example, respiratory bellows may not provide reliable respiratory signals for small children. The ECG signal can be corrupted due to RF/gradient interference and magnetohydrodynamic effects (6).

By modifying standard MR pulse sequences, motion information can be extracted without the use of external motion monitoring devices. This can be achieved by adding navigator echoes throughout the scan, or using self-navigating pulse sequences (7–26). The measured motion is usually perfectly synchronized with the acquired MR data for effective respiratory gating/triggering or cardiac gating/triggering. Some self-navigating techniques, such as Butterfly (27) and radial trajectories (28, 29), have been clinically evaluated. Effective and robust motion compensation has been reported in different clinical applications, including free-breathing abdominal MRI and cardiac MRI (30–33).

Dense coil arrays with small coil elements and high channel counts can provide additional information about subject motion (34–36). For self-navigating pulse sequences, each coil element can generate a motion estimate within a local region. For example, respiratory motion and cardiac motion can be difficult to directly separate using a single-channel receiving coil in free-breathing cardiac MRI. However, with coil arrays, individual coil elements may be manually selected for respiratory motion or cardiac motion estimation due to localized coil sensitivities (37). Virtual coils with desired coil sensitivity for respiratory motion or cardiac motion estimation can also be synthesized from the original coil arrays (38). It is possible to separate respiratory motion and cardiac motion by filtering based on their intrinsic frequency differences as well (28, 39, 40). In all of these approaches, the performance of the corresponding motion compensation/correction highly depends on the chosen motion estimate. Manual selection of the desired motion estimate can guarantee ideal motion compensation/correction, but is not viable for routine clinical use. Alternatively, automatic averaging of motion estimates from all coils can be applied (30). Though its performance can be compromised when undesired motion estimates are included.

In this work, a robust motion estimation method using coil clustering is proposed for 3D free-breathing body MRI. We investigate whether the proposed method can automatically determine the dominant motion by selecting the motion estimates from a subset of coil elements in dense coil arrays. For abdominal imaging, we explore whether automated coil clustering can effectively estimate respiratory motion. We then combine coil clustering with

an appropriate filter design to determine the feasibility of estimating both cardiac motion and respiratory motion for free-breathing cardiac cine MRI.

Methods

All imaging was performed with free breathing in this work. A modified self-navigating sequence (Butterfly) was used to generate motion estimates. Butterfly is a modification of the Cartesian trajectory, with the prewinder gradients traversing the same trajectory at the beginning of each phase encode. With the traversing trajectory alternating at different directions, translational motion estimation along all three directions (superior/inferior: S/I, right/left: R/L, and anterior/posterior: A/P) can be achieved for 3D acquisitions. Detailed descriptions of Butterfly can be found in reference (36,41).

Robust motion estimation using coil clustering

For MRI data acquisition with dense coil arrays, individual coil elements only provide motion estimates within small regions due to localized coil sensitivities. Motion estimates from different coil elements can vary significantly, and do not individually represent the dominant motion within the entire imaging volume. For example, the S/I motion estimates from a 32-channel coil during an abdominal MRI scan are shown in Fig. 1(a): only one motion estimate from three selected coils accurately represents the dominant respiratory motion. In fact, only a subset of coils can effectively track the dominant motion. This subset of coils is referred to as a *coil cluster* for the rest of the manuscript.

To automatically determine the coil cluster that represents the dominant motion, a coil clustering technique is proposed. The coil clustering algorithm is illustrated in Fig. 1. Assume that there is one dominant motion within the imaging volume (e.g., respiration for abdominal imaging), and this dominant motion is accurately measured by multiple coils. Define S a coil cluster, d_i the motion estimate from coil i, and N the total number of coils used for data acquisition. Then the problem of finding the coil cluster that represents the dominant motion can be equivalently formulated as:

$$\begin{aligned} \underset{S\subset\{1,2,\ldots,N\}}{\text{maximize}} \quad & |S| \\ \text{subject to} \quad & |\rho(d_i,d_j)|>t, \forall i,j\in S \end{aligned} \tag{1}$$

where $|S|$ is the number of coils (or cardinality) of the coil cluster, $\rho(d_i, d_j)$ is the correlation coefficient (range from −1 to 1) between motion estimates from coil i and coil j, and t is the threshold of the correlation coefficient.

This problem is in fact NP-hard. However, spectral clustering can be used to approximately solve this problem (42). The major steps in the proposed algorithm are listed below:

1. Calculation of the correlation matrix C of the motion estimates (navigator correlation matrix). Define $C(i, j) = \rho(d_i, d_j)$, $\forall i, j \in \{1, 2, \ldots, N\}$. An example of the navigator correlation matrix is shown in Fig. 1(b).

2. Construction of the correlation graph G. This step requires an entry-wise thresholding operation (shown in Fig. 1(c)).

$$G(i,j)=\begin{cases} 1, \text{ if } |C(i,j)| \geq t \\ 0, \text{ otherwise} \end{cases} \quad (2)$$

Note that the correlation graph highly depends on the chosen threshold t. The nonzero entries in Fig. 1(c) represent navigator pairs whose correlation coefficient is above the threshold.

3. Eigenvalue decomposition of the correlation graph G.

$$G=USU^T \quad (3)$$

As shown in Fig. 1(d), the eigenvalues in S decay dramatically, which represents the low-rank property of G.

4. Coil clustering based on the eigenvector corresponding to the largest eigenvalue. Note that this eigenvector (highlighted in Fig. 1(d)) only has a few significant (non-zero) entries. This essentially represents the support of the coil cluster. Define u_1 the eigenvector corresponding to the largest eigenvalue of G. The coil cluster can be found by another thresholding operation:

$$\begin{cases} \text{if } |u_1(i)| \geq \epsilon, \ i \in S \\ \text{if } |u_1(i)| < \epsilon, \ i \notin S \end{cases}, \ \forall i \in \{1,2,\ldots,N\}, \quad (4)$$

where ϵ is the threshold for the eigenvector u_1. In this work, ϵ was empirically chosen as 0.1 and kept constant for all studies. The rank of the correlation graph of the final coil cluster should be 1 (shown in Fig. 1(e)).

After these steps, the coil cluster S can be found. The final motion estimate can be generated by averaging of the motion estimates within the coil cluster. If the number of coils within the coil cluster is only one, the motion estimate is assumed unreliable and set to zero. Note that sometimes the motion estimates within the coil cluster can be negatively correlated. That is, the motion estimates from two different coils can represent translational motion in opposite directions (as shown in Supporting Figure S1). Therefore, motion estimates within the coil cluster need to be first automatically aligned based on the sign of the correlation coefficient before averaging so that they do not cancel out.

For 3D abdominal MRI using Butterfly, motion estimates in the S/I, A/P and R/L directions can all be acquired. The proposed coil clustering method should be applied separately in each direction for accurate motion estimation. For further motion compensation/correction, motion estimates in different directions can be used individually or combined (e.g., square root of sum of squares).

Motion estimation for 3D free-breathing cardiac MRI

For free-breathing cardiac MRI, the motion estimates usually contain both respiratory motion and cardiac motion. Therefore, additional motion estimation processing steps are required to separate these two types of motion. In this work, bandpass filtering (40) was applied. Based on empirical studies, the subject heart rate was assumed to range from 70% to 140% of the heart rate recorded prior to the cardiac exam or estimated from the motion estimates (28). For example, if the heart rate prior to the exam is 60 beats per minute (BPM), then the heart rate during the cardiac exam is assumed to range from 42 to 84 BPM. To extract cardiac motion, a bandpass filter was designed according to this heart rate range. A Kaiser-windowed finite impulse response filter of order 500 and $\beta = 4.5$ was applied. Bandpass filtering was performed in both the forward and reverse directions to yield zero group delay (18). The remaining lower-frequency signal is assumed to be the respiratory motion. An example of the Butterfly navigators from a 3D phase-contrast cardiac cine scan is shown in Fig. 2. Coil clustering can be applied separately on both the cardiac motion estimates and respiratory motion estimates for further motion compensation/correction.

In vivo studies

To investigate the feasibility of the proposed method in a clinical setting, in vivo free-breathing abdominal and cardiac studies were carried out. For each study, ten subjects referred for MRI of the respective body parts were recruited at our institution. Subject demographics in these studies are listed in Supporting Tables S1-S3. All imaging was performed on a 3T GE scanner (GE Healthcare, Waukesha, WI) using a 32-channel cardiac coil. Both studies were approved by the institutional review board, and informed consent/assent was obtained prior to imaging.

Self-navigated 3D free-breathing abdominal imaging—To evaluate the performance of the proposed method in abdominal imaging, 3D coronal free-breathing dynamic contrast-enhanced MRI was performed using a modified RF-spoiled gradient echo sequence with self-navigation, fat saturation and variable density sampling patterns (30, 43). The acquisition parameters were flip angle 15°, TE 1.2–1.4 ms (partial echo), TR 3.2–3.4 ms, bandwidth ± 100 kHz, slice thickness (A/P) 2.0–3.0 mm (mean: 2.4 mm), S/I field of view (FOV) 26–42 cm, spatial resolution 0.9–1.3 mm (S/I) and 1.2–1.9 mm (R/L), and frame rate 8.2–11.7 s. Gadobutrol (Bayer Healthcare, Leverkusen, Germany) injection was initiated at the end of the first frame, and 18 frames in total were acquired. Respiratory bellows signal during the scan was recorded. Most subjects were sedated in this study.

Butterfly motion estimates in the S/I, R/L and A/P directions were calculated for each coil element. The reference motion estimate that best represents respiratory motion was manually selected from the coil arrays. The correlation coefficients of the motion estimates between the reference and different methods were calculated. To determine the optimal threshold t in the proposed coil clustering method, three representative patients with different age and size were first selected. Coil clustering with twenty different thresholds in the range of [0, 0.99] were performed on the three subjects. The number of coils selected and the corresponding correlation coefficients with different thresholds were recorded and

compared. Next, the proposed method with empirically chosen thresholds $t = 0{:}95$ and $t = 0{:}90$ was performed. Averaged motion estimate from all coils was also computed.

Self-navigated 3D free-breathing cardiac imaging—To evaluate the performance of the proposed method in cardiac imaging, 3D phase-contrast cardiac cine MRI was performed using a modified RF-spoiled gradient echo sequence with self-navigation, unbalanced flow encoding and variable density sampling pattern (41). Imaging parameters were flip angle 15°, TE 1.8 ms, TR 9.1 ms, velocity encoding range (VENC) 250 cm/s, and bandwidth ± 83.33 kHz, slice thickness (S/I) 1.0–2.0 mm (mean: 1.5 mm), R/L FOV 20–30 cm (mean: 25 cm), and matrix 320 × 224 × 120. Ferumoxytol (AMAG Pharmaceuticals, Waltham, MA, USA) was injected prior to the study for blood pool enhancement. Most subjects were sedated in this study. The acquisition was performed with prospective ECG triggering. The ECG trigger points were recorded and used as the reference in the following evaluations.

Butterfly motion estimates in the S/I, R/L and A/P directions were calculated for each coil element. Cardiac motion and respiratory motion were separated using bandpass filtering described previously. The proposed coil clustering method with empirically chosen $t = 0{:}95$ and $t = 0{:}90$ was performed to generate a robust motion estimate. An averaged motion estimate from all coils was also computed. Similar to the previous abdominal imaging study, respiratory motion was evaluated with manual selection as the reference. To assess the cardiac motion estimates, self-gated cardiac triggered points were calculated using a template matching algorithm for cardiac synchronization (17). To quantify the difference between self-gating and ECG gating, temporal variability (TV) and mean trigger delay (MTD) were used. TV between the self-gating trigger points $\boldsymbol{S}$ and a set of recorded ECG R-wave trigger points $\boldsymbol{R}$ is defined by the following equation:

$$\mathrm{TV}=\sqrt{\frac{1}{N-1}\sum_{n=1}^{N}((S_n-R_n)-\mathrm{MTD})^2}, \quad (5)$$

where N is the total number of cardiac cycles and MTD is the mean trigger delay,

$$\mathrm{MTD}=\frac{1}{N}\sum_{n=1}^{N}(S_n-R_n)\,. \quad (6)$$

All signal processing and image reconstruction were conducted in MATLAB (MathWorks, Natick, MA).

Results

Self-navigated 3D free-breathing abdominal imaging

The results of threshold selection analysis for coil clustering on three subjects are shown in Supporting Figure S2. A range of 0.9 to 0.95 achieved near optimal correlation coefficient in

all cases. Different motion estimation processing methods from a representative dataset are shown in Fig. 3. As the threshold t decreased from 0.95 to 0.90, more coils were selected for the coil cluster (Fig. 3(a, b)). The averaged motion estimates from coil clustering resembled that with manual selection. The amplitude of the averaged motion estimate within the coil cluster decreased with the reduced threshold t in the S/I and A/P direction. Note that different coils were selected for motion estimation in different directions. The S/I motion estimates selected by the proposed coil clustering were mostly from coil elements near the diaphragm, where pencil beam navigators are commonly used. Respiratory motion was also observed in the R/L and A/P direction, though the amplitude of the estimated motion was smaller in the R/L and A/P direction compared to S/I. Respiratory bellows signal during the scan was also recorded. However, as shown in Fig. 3(c), the shape of the respiratory bellows signal did not correlate well with the manually selected motion estimate, likely due to poor positioning of the bellows. Retrospective respiratory gating based on the motion estimates from different methods was performed and compared in Fig. 3(d). Similar image quality was observed between manual selection and coil clustering.

The results of different motion estimation processing methods compared to manual selection on all subjects are shown in Supporting Table S1. A correlation coefficient smaller than 0.9 compared to the reference manual selection (highlighted in bold in Supporting Table S1) was considered failed motion estimation. Coil clustering achieved robust motion estimation in the S/I direction for all the subjects, while averaging over all coils was more likely to fail in the R/L direction. Coil clustering with $t = 0.95$ and $t = 0.90$ yielded similar motion estimation performance.

Self-navigated 3D free-breathing cardiac imaging

The results of the respiratory motion analysis in the cardiac imaging study are shown in Supporting Table S2. Similar to abdominal imaging, coil clustering was able to consistently find a respiratory motion estimate that highly correlated with the manual selection in the S/I direction, while averaging over all coils did not provide robust motion estimation for some subjects in this study, especially in the R/L direction. Coil clustering with $t = 0.95$ performed slightly better than with $t = 0.90$ for respiratory motion estimation in this study.

An example of the estimated cardiac motion by coil clustering and averaging over all coils is shown in Fig. 4. Coil clustering achieved robust self-gating and matched well with the recorded ECG triggers (with noticeable MTD in the R/L and A/P direction). However, the estimated cardiac motion by averaging over all coils was corrupted in the S/I and A/P direction, which led to inaccurate self-gating and unreliable triggered points. We labeled this situation as failed self-gating, and the corresponding TV value was not calculated. An example of ECG-gated and self-gated cardiac cine reconstruction is shown in Fig. 5. Similar image quality was achieved by both methods.

The results of the TV analysis of all subjects are shown in Supporting Table S3. Coil clustering succeeded to find trigger points for all cases in all three directions. However, averaging over all coils failed in some cases. The averaged TV was smaller for the coil clustering method with $t = 0.90$ than $t = 0.95$. The R/L direction provided the most reliable trigger points (averaged TV = 17.5 ms).

Discussion

The proposed coil clustering method can achieve robust motion estimation for dense coil arrays. It enabled self-navigated free-breathing MRI acquisition for both abdominal and cardiac MRI without using any external motion monitoring devices. The automatically determined motion estimate by coil clustering matched the manually selected motion estimate or recorded ECG signal for all subjects recruited in this work. Fully automated image reconstruction with motion compensation/correction can be achieved using coil clustering.

The major parameter in the proposed method is the threshold of the correlation coefficient of different navigators in Eq. 1. As the threshold reduces, more coils will be selected. Averaging of all coils can be considered as the extreme case of setting the threshold to zero. As shown in the experiments, a threshold between 0.95 and 0.90 has consistently provided acceptable results, and is recommended for abdominal and cardiac MRI. As recommended by (42), the other parameter in Eq. 4 was empirically chosen as 0.1 and kept constant in this work.

Because of the Butterfly technique used in this work, translational motion in three directions (S/I, A/P, and R/L) was all estimated. Although only Butterfly was used in this study, the proposed method is expected to work with other methods that can generate coil-by-coil motion estimates. For abdominal MRI, the S/I direction is recommended for respiratory motion estimation; for cardiac MRI, R/L is recommended for cardiac motion estimation. In some cases, the coils selected for cardiac motion can also be selected for respiratory motion. However, based on our experience, the coil clusters selected for respiratory motion and cardiac motion do not correlate much. The coil cluster pattern varies by subjects and motion types and directions.

The focus of this work is to automatically determine the dominant motion within large imaging volumes. Although averaging within the coil cluster was used to generate the final motion estimate, other operations can be applied as well. For example, the motion estimate with the maximum amplitude within the coil cluster can be selected, which in fact is expected to be exactly the manually selected motion estimate. For the retrospective respiratory gating and cardiac gating applied in this work, different methods of generating the final motion estimate from the coil cluster are not expected to significantly impact the results. They will be further investigated for other motion compensation/correction in the future work.

A limitation of this work is that the proposed method was only evaluated using quantitative objective metrics. Subjective image quality comparison by radiologists is beyond the scope of this work, and will be the subject of future work. Manual motion estimate selection was served as the reference for evaluating respiratory motion. Depending on the selected reference, the correlation coefficient between the reference and motion estimates by other methods can vary slightly. Although respiratory bellows could be used, we were unable to obtain reliable respiratory bellows signals for young children.

The proposed motion estimation method for free-breathing cardiac MRI requires prior knowledge of the subject heart rate. The filter design to separate cardiac and respiratory motion highly depends on this input. The cardiac datasets in this work were acquired with prospective ECG triggering, and the heart rates were already available. If not measured, the heart rate can also be approximately estimated by a simple frequency analysis of the raw navigators (28, 39, 40). The use of a passband filter to extract cardiac motion may affect cardiac gating performance in cases of arrhythmia. Further investigation on the performance with different filter designs in cases of arrhythmia will also be the subject of future work.

Conclusion

A robust motion estimation method using coil clustering for free-breathing body MRI has been presented. The proposed method can automatically detect the dominant motion within the imaging volume for dense coil arrays. The feasibility of such automated coil selection for navigation was demonstrated in a pilot study on various in vivo datasets for both respiratory motion estimation and cardiac motion estimation. It has enabled free-breathing abdominal or cardiac MRI without the need for external motion monitoring devices, and fully automated motion compensation/correction.

Supplementary Material

Refer to Web version on PubMed Central for supplementary material.

Acknowledgments

The authors thank Marcus Alley for help with the pulse sequence implementation, and Paul Calderon for help with the manuscript preparation.

This work was supported by NIH grants R01 EB009690, R01 EB019241, P41 EB015891, the Tashia and John Morgridge Faculty Scholars Fund, and GE Healthcare.

References

1. Kim B, Angthong W, Jeon Y, Semelka R. Body MR imaging: fast, efficient, and comprehensive. Radiol Clin North Am. 2014; 52:623–636. [PubMed: 24889164]
2. Ehman R, McNamara M, Pallack M, Hricak H, Higgins C. Magnetic resonance imaging with respiratory gating: techniques and advantages. AJR AM J Roentgenol. 1984; 143:1175–1182. [PubMed: 6333787]
3. Lanzer P, Botvinick E, Schiller N, Crooks L, Arakawa M, Kaufman L, Davis P, Herfkens R, Lipton M, Higgins C. Cardiac imaging using gated magnetic resonance. Radiology. 1984; 150:121–127. [PubMed: 6227934]
4. Fletcher B, Jacobstein M, Nelson A, Riemenschneider T, Alfidi R. Gated magnetic resonance imaging of congenital cardiac malformations. Radiology. 1984; 150:137–140. [PubMed: 6689753]
5. Smith M, Ridgway J, Brydon J, Been M, Douglas R, Kean D, Muir A, Best J. ECG-gated T_1 images of the heart. Phys Med Biol. 1986; 31:771–778. [PubMed: 3749262]
6. Nacif M, Zavodni A, Kawel N, Choi E, Lima J, Bluemke D. Cardiac magnetic resonance imaging and its electrocardiographs (ECG): tips and tricks. Int J Cardiovasc Imaging. 2012; 28:1465–1475. [PubMed: 22033762]
7. Ehman R, Felmlee J. Adaptive technique for high-definition MR imaging of moving structures. Radiology. 1989; 173:255–263. [PubMed: 2781017]

8. Wang Y, Grimm R, Felmlee J, Riederer S, Ehman R. Algorithms for extracting motion information from navigator echoes. Magn Reson Med. 1996; 36:117–123. [PubMed: 8795030]
9. Pipe J. Motion correction with PROPELLER MRI: application to head motion and free-breathing cardiac imaging. Magn Reson Med. 1999; 42:963–969. [PubMed: 10542356]
10. Welch E, Manduca A, Grimm R, Ward H, Jack C Jr. Spherical navigator echoes for full 3D rigid body motion measurement in MRI. Magn Reson Med. 2002; 47:32–41. [PubMed: 11754440]
11. Stehning C, Böornert P, Nehrke K, Eggers H, Stuber M. Free-breathing whole-heart coronary MRA with 3D radial SSFP and self-navigated image reconstruction. Magn Reson Med. 2005; 54:476–480. [PubMed: 16032682]
12. Brau A, Brittain J. Generalized self-navigated motion detection technique: Preliminary investigation in abdominal imaging. Magn Reson Med. 2006; 55:263–270. [PubMed: 16408272]
13. Lai P, Larson A, Bi X, Jerecic R, Li D. A dual-projection respiratory self-gating technique for whole-heart coronary MRA. J Magn Reson Imaging. 2008; 28:612–620. [PubMed: 18777542]
14. Mendes J, Parker D. Intrinsic detection of motion in segmented sequences. Magn Reson Med. 2011; 65:1084–1089. [PubMed: 21413072]
15. Larson A, Kellman P, Arai A, Hirsch G, McVeigh E, Li D, Simonetti O. Preliminary investigation of respiratory self-gating for free-breathing segmented cine MRI. Magn Reson Med. 2005; 53:159–168. [PubMed: 15690515]
16. Leung A, Paterson I, Thompson R. Free-breathing CINE MRI. Magn Reson Med. 2008; 60:709–717. [PubMed: 18727100]
17. Nijm G, Sahakian A, Swiryn S, Carr J, Sheehan J, Larson A. Comparison of self-gated cine MRI retrospective cardiac synchronization algorithms. J Magn Reson Imaging. 2008; 28:767–772. [PubMed: 18777546]
18. Ingle R, Santos J, Overall W, McConnell M, Hu B, Nishimura D. Self-gated fat-suppressed cardiac CINE MRI. Magn Reson Med. 2015; 73:1764–1774. [PubMed: 24806049]
19. Lai P, Bi X, Jerecic R, Li D. A respiratory self-gating technique with 3D-translation compensation for free-breathing whole-heart coronary MRA. Magn Reson Med. 2009; 62:731–738. [PubMed: 19526514]
20. Pfeuffer J, Van de Moortele P, Ugurbil K, Hu X, Glover G. Correction of physiologically induced global off-resonance effects in dynamic echo-planar and spiral functional imaging. Magn Reson Med. 2002; 47:344–353. [PubMed: 11810679]
21. Usman M, Atkinson D, Kolbitsch C, Schaeffter T, Prieto C. Manifold learning based ECG-free free-breathing cardiac CINE MRI. J Magn Reson Imaging. 2015; 41:1521–1527. [PubMed: 25124545]
22. Uribe S, Muthurangu V, Boubertakh R, Schaeffter T, Razavi R, Hill D, Hansen M. Whole-heart cine MRI using real-time respiratory self-gating. J Magn Reson Imaging. 2007; 57:606–613.
23. Graesslin, I.; Glaesel, D.; Böornert, P.; Dingemans, H.; Mens, G.; Harvey, P. An alternative concept of selfnavigation for patient respiration monitoring; Proceedings of the 15th Annual Meeting of ISMRM; Berlin. 2007. p. 867
24. Larson A, White R, Laub G, McVeigh E, Li D, Simonetti O. Self-gated cardiac cine MRI. Magn Reson Med. 2004; 51:93–102. [PubMed: 14705049]
25. Coppo S, Piccini D, Bonanno G, Chaptinel J, Vincenti G, Feliciano H, van Heeswijk R, Schwitter J, Stuber M. Free-running 4D whole-heart self-navigated golden angle MRI: initial results. Magn Reson Med. 2014; doi: 10.1002/mrm.25523
26. Stainsby J, Susan M, Flexman M, Wright G. Real-time magnetic resonance with physiologic monitoring for improved scan localization. Magn Reson Med. 2005; 53:954–959. [PubMed: 15799048]
27. Lustig, M.; Cunningham, C.; Daniyalzade, E.; Pauly, J. Butterfly: a self-navigating Cartesian trajectory; Proceedings of the 15th Annual Meeting of ISMRM; Berlin. 2007. p. 865
28. Feng L, Axel L, Chandarana H, Block K, Sodickson D, Otazo R. XD-GRASP: golden-angle radial MRI with reconstruction of extra motion-state dimensions using compressed sensing. Magn Reson Med. 2015; doi: 10.1002/mrm.25665

29. Piccini D, Littmann A, Nielles-Vallespin S, Zenge M. Respiratory self-navigation for whole-heart bright-blood coronary MRI: methods for robust isolation and automatic segmentation of the blood pool. Magn Reson Med. 2012; 68:571–579. [PubMed: 22213169]
30. Zhang T, Cheng J, Potnick A, Barth R, Alley M, Uecker M, Lustig M, Pauly J, Vasanawala S. Fast pediatric 3D free-breathing abdominal dynamic contrast enhanced MRI with high spatiotemporal resolution. J Magn Reson Imaging. 2015; 41:460–473. [PubMed: 24375859]
31. Chandarana H, Block K, Rosenkrantz A, Lim R, Kim D, Mossa D, Babb J, Kiefer B, Lee V. Free-breathing radial 3D fat-suppressed T1-weighted gradient echo sequence: a viable alternative for contrast-enhanced liver imaging in patients unable to suspend respiration. Invest Radiol. 2011; 46:648–653. [PubMed: 21577119]
32. Piccini D, Monney P, Sierro C, Coppo S, Bonanno G, van Heeswijk R, Chaptinel J, Vincenti G, de Blosi J, Koestner S, Rutz T, Littmann A, Zenge M, Schwitter J, Stuber M. Respiratory self-navigated post contrast whole-heart coronary MR angiography: initial experience in patients. Radiology. 2014; 270:378–386. [PubMed: 24471387]
33. Cheng J, Zhang T, Ruangwattanapaisarn N, Alley M, Uecker M, Pauly J, Lustig M, Vasanawala S. Free-breathing pediatric MRI with nonrigid motion correction and acceleration. J Magn Reson Imaging. 2014; doi: 10.1002/jmri.24785
34. Hu P, Hong S, Moghari M, Goddu B, Goepfert L, Kissinger K, Hauser T, Manning W, Nezafat R. Motion correction using coil arrays (MOCCA) for free-breathing cardiac cine MRI. Magn Reson Med. 2011; 66:467–475. [PubMed: 21773986]
35. Liu J, Drangova M. Combination of multidimensional navigator echoes data from multidimensional RF coil. Magn Reson Med. 2010; 64:1208–1214. [PubMed: 20564594]
36. Cheng J, Alley M, Cunningham C, Vasanawala S, Pauly J, Lustig M. Nonrigid motion correction in 3D using autofocusing with localized linear translations. Magn Reson Med. 2012; 68:1785–1797. [PubMed: 22307933]
37. Feng L, Axel L, Latson L, Xu J, Sodickson D, Otazo R. Compressed sensing with synchronized cardio-respiratory sparsity for free-breathing cine MRI: initial comparative study on patients with arrhythmias. J Cardiov Magn Reson. 2014; 16(Suppl 1):O17.
38. Shi, X.; Cheng, J.; Lustig, M.; Pauly, J.; Vasanawala, S. Virtual coil navigator: a robust localized motion estimation approach for free-breathing cardiac MRI; Proceedings of the 23rd Annual Meeting of ISMRM; Toronto. 2015. p. 811
39. Buehrer M, Curcic J, Boesiger P, Kozerke S. Prospective self-gating for simultaneous compensation of cardiac and respiratory motion. Magn Reson Med. 2008; 60:683–690. [PubMed: 18727084]
40. Liu J, Spincemaille P, Codella N, Nguyen T, Prince M, Wang Y. Respiratory and cardiac self-gated free-breathing cardiac CINE imaging with multiecho 3D hybrid radial SSFP acquisition. Magn Reson Med. 2010; 63:1230–1237. [PubMed: 20432294]
41. Cheng, J.; Alley, M.; Zhang, T.; Lai, P.; Tamir, J.; Uecker, M.; Pauly, J.; Lustig, M.; Vasanawala, S. Soft-gated accelerated Cartesian 4D flow imaging with intrinsic navigation; Proceedings of the 23rd Annual Meeting of ISMRM; Toronto. 2015. p. 451
42. Shi J, Malik J. Normalized cuts and image segmentation. IEEE Trans Pattern Anal Mach Intell. 2000; 22:888–905.
43. Cheng, J.; Zhang, T.; Alley, M.; Lustig, M.; Vasanawala, S.; Pauly, J. Variable-density radial view-ordering and sampling for time-optimized 3D Cartesian imaging; Proceedings of ISMRM Workshop on Data Sampling & Image Reconstruction; Sedona, AZ. 2013.

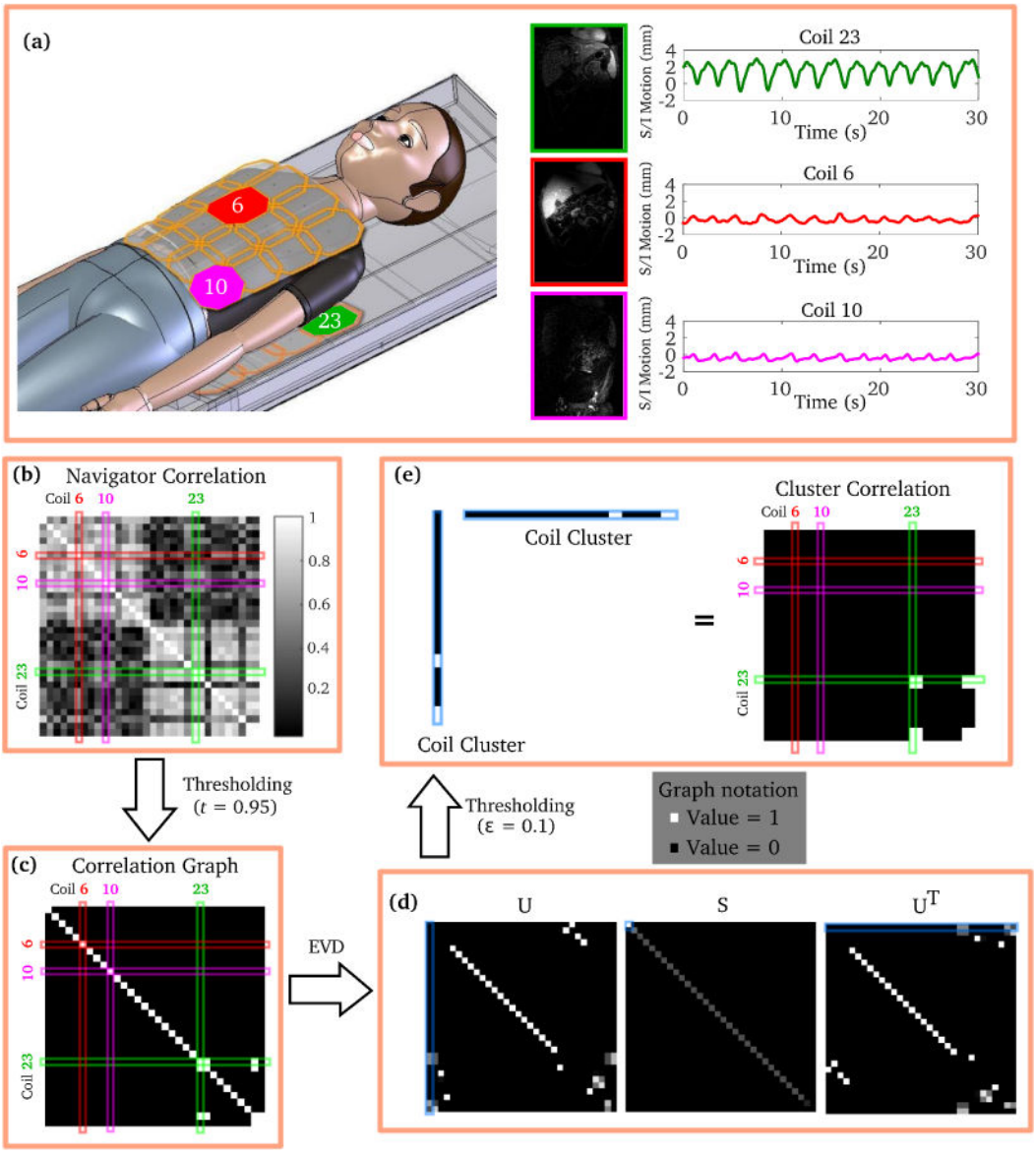

Figure 1.

Demonstration of the coil clustering method. (a) S/I motion estimates (navigators) from three individual coil elements (red, pink, and green) vary significantly due to localized coil sensitivities. The proposed method consists of the following major steps to automatically find a subset of coils to determine the dominant motion: (b) calculation of the correlation matrix of the navigators; (c) construction of a correlation graph by thresholding the correlation matrix; (d) eigenvalue decomposition (EVD) of the correlation graph; (e) thresholding of the eigenvector corresponding to the largest eigenvalue. The significant entries in the thresholded eigenvector represent the selected coils in the coil cluster. The correlation graph of the coil cluster shows good approximation of the highly correlated coil subset in (c).

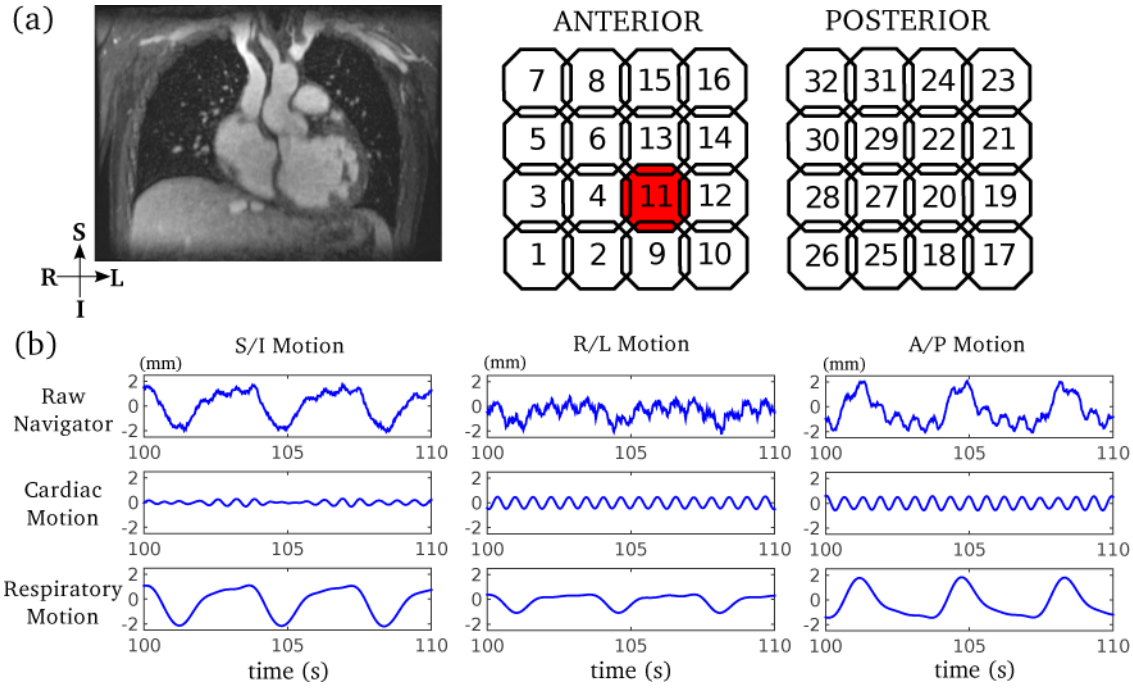

Figure 2.

Example of 3D motion estimates in free-breathing cardiac MRI. (a) Typical imaging volume of a 3D phase-contrast cardiac MRI; (b) 3D motion estimates (navigators) from an example coil element (highlighted in (a)) are shown to demonstrate the separation of cardiac motion and respiratory motion using bandpass filtering. The raw motion estimate contains both cardiac motion and respiratory motion, which can be separated by bandpass filtering prior to coil clustering.

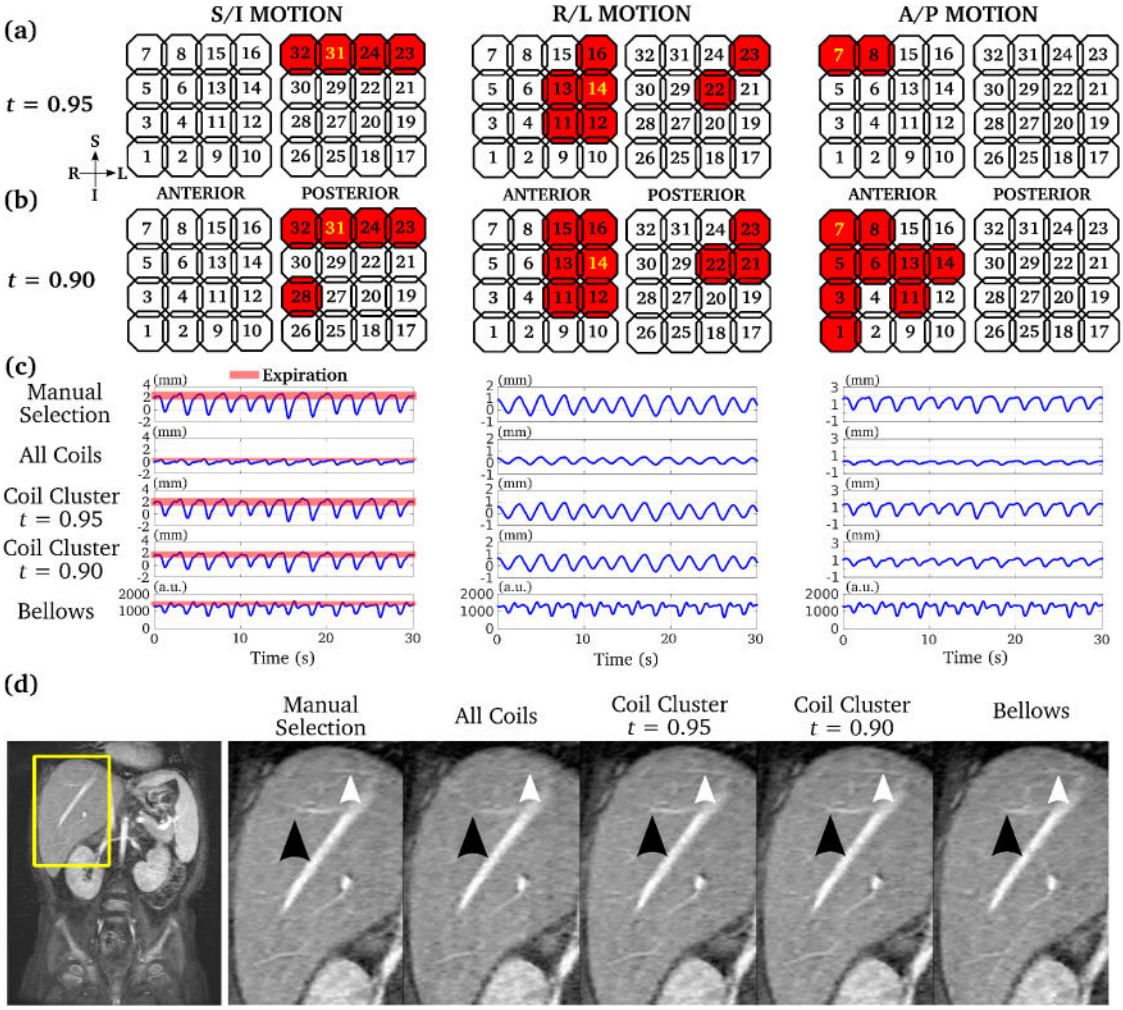

Figure 3.

Comparison of 3D motion estimates for abdominal MRI using manual selection, averaging of all coils, coil clustering, and respiratory bellows. Selected coil elements with two different coil clustering parameters ($t = 0.95$ and 0.90) are highlighted by red in (a) and (b) respectively. The manually selected coil element is highlighted by yellow in (a) and (b). As the threshold t decreased, more coils were selected by coil clustering. The corresponding motion estimates by all methods are shown in (c). Retrospective respiratory gating was performed using each of the motion estimate in (c), and the corresponding images are shown in (d). The proposed coil clustering method achieved very similar image quality compared to that with manual selection, with sharp delineation of branches of the heptic veins (arrows).

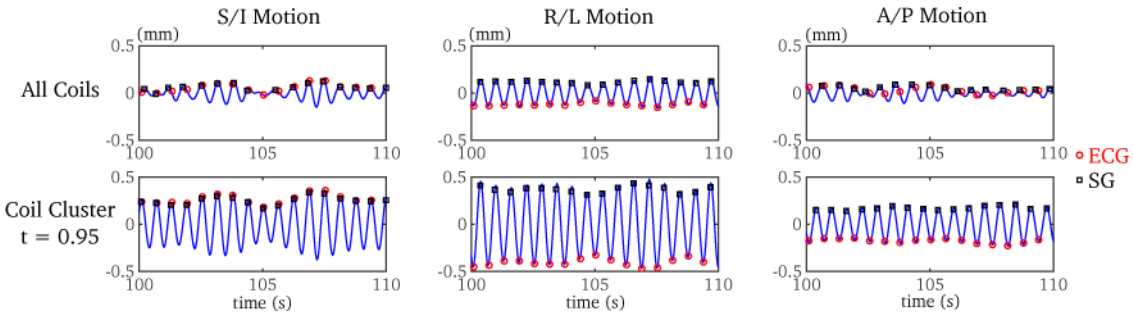

Figure 4.

Comparison of self gating (SG) methods using averaged cardiac motion estimates from all coils and cardiac motion estimate by coil clustering of a 4-year-old subject. Both the recorded ECG trigger points and the self-gated trigger points using a template matching algorithm are shown. In the S/I and A/P directions, the self-gating method using an averaged motion estimate from all coils failed to provide accurate cardiac trigger points. However, coil clustering provided robust self-gated triggered points in all three directions. Note that mean trigger delay (MTD) varied at different directions. The temporal variability (TV) with coil clustering was 13.8 ms, 11.7 ms, and 12.2 ms, for the S/I, R/L and A/P directions respectively.

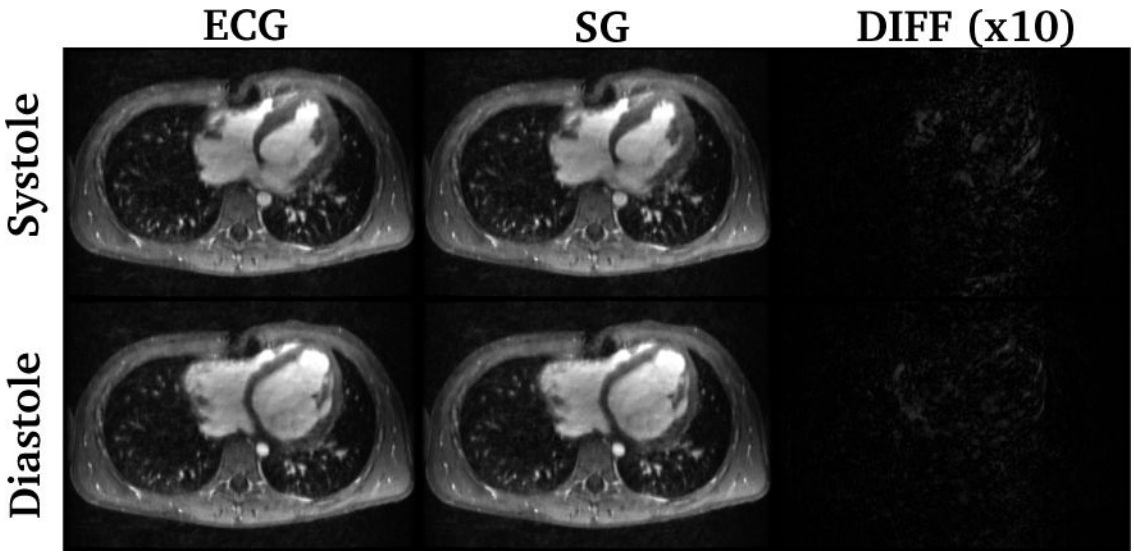

Figure 5.

Example of cardiac cine MRI retrospectively temporally-interpolated using the recorded ECG signal and the proposed self-gating method (SG). Systolic and diastolic images of a 9.5-year-old subject are shown. The differences (scaled by a factor of 10) between images with two cardiac trigger methods are also shown. Similar image quality was observed for both methods. All images are displayed with the same window width and window level. The temporal variability was 20.7 ms.